Materials Horizons

High Photoluminescence Quantum Yield Near-Infrared Emission from a Lead-Free Ytterbium-Doped Double Perovskite

Journal:	*Materials Horizons*
Manuscript ID	MH-COM-04-2022-000483.R1
Article Type:	Communication
Date Submitted by the Author:	01-Jun-2022
Complete List of Authors:	Tran, Minh; New York University Tandon School of Engineering, Chemical and Biomolecaulr Engineering Department Cleveland, Iver; New York University Tandon School of Engineering, Chemical and Biomolecaulr Engineering Geniesse, Joseph; New York University Tandon School of Engineering, Chemical and Biomolecaulr Engineering Aydil, Eray; New York University Tandon School of Engineering, Department of Chemical Engineering and Biomolecular Engineering

New Concept Statement:

We demonstrate that Yb^{3+} ions substitute into the double perovskite structure of $Cs_2AgBiBr_6$, specifically into the $AgBr_6^{5-}$ and/or $BiBr_6^{3-}$ octahedra, leading to a lead-free halide perovskite that converts ultraviolet and blue photons to near infrared (NIR) photons with record efficiency. Specifically, we report record NIR photoluminescence quantum yields (PLQY) as high as 82.5% for excitation energies above the bandgap (>2.2 eV). This record nearly triples the previous PLQY record (28%) from lead-free Yb-doped halide perovskites. We also settle a debate on the origin of an orange emission from this material, showing conclusively that it is due to a defect and not band-edge transition or self-trapped excitons as previously hypothesized.

This is an important finding because Yb is a well-known luminophore for red shifting the solar spectrum entering a solar cell by creating NIR photons from blue photons via down conversion or quantum cutting to increase solar cell efficiencies. Quantum cutting is a process wherein one UV-blue photon is converted to two NIR photons. Indeed, Yb-doped $CsPb(Cl,Br)_3$ has been shown to exhibit quantum cutting with PLQY of 190%, however, lead is toxic. Our work is differentiated from existing research because our material does not contain lead and exhibits the highest NIR PLQY from any Yb-doped lead-free halide perovskite.

COMMUNICATION

High Photoluminescence Quantum Yield Near-Infrared Emission from a Lead-Free Ytterbium-Doped Double Perovskite

Minh N. Tran, [a] Iver J. Cleveland [a] Joseph R. Geniesse [a] and Eray S. Aydil *[a]

Received 00th January 20xx,
Accepted 00th January 20xx

DOI: 10.1039/x0xx00000x

When excited by photons with energies greater than 2.2 eV, the bandgap energy, Yb-doped $Cs_2AgBiBr_6$ thin films synthesized via physical vapor deposition emit strong near-infrared luminescence centered at ~ 1.24 eV via the Yb^{3+} $^2F_{5/2} \rightarrow {}^2F_{7/2}$ electronic transition. Robust, reproducible, and stable photoluminescence quantum yields (PLQY) as high as 82.5% are achieved with $Cs_2AgBiBr_6$ films doped with 8% Yb. This high PLQY indicates facile and efficient energy transfer from the perovskite host, $Cs_2AgBiBr_6$, to Yb, making $Cs_2AgBiBr_6$ the most promising lead-free down-conversion material.

Redshifting the solar spectrum entering a solar cell by creating near-infrared (NIR) photons from ultraviolet (UV) and blue photons via luminescence down conversion can increase the solar cell's efficiency. Shifting the UV and blue spectrum to NIR reduces thermal losses and the recombination of electron-hole pairs generated from shallow light absorption near interfaces. Ytterbium (Yb) is a well-known luminophore for solar spectral shifting because the Yb^{3+} emission via $^2F_{5/2} \rightarrow {}^2F_{7/2}$ electronic transition at 1.24 eV is close to the bandgap of silicon (~ 1.1 eV) and copper indium gallium diselenide, CIGS (1.0-1.2 eV).[1] Typically, Yb is doped into a host, which absorbs in the UV and visible regions of the electromagnetic spectrum and transfers energy to the Yb^{3+}, exciting it from the $^2F_{7/2}$ ground state to the $^2F_{5/2}$ state. The excited Yb^{3+} emits NIR photons at ~1.24 eV upon relaxation. Thus, depositing a layer of a Yb-doped film with high photoluminescence quantum yield (PLQY) on top of a silicon solar cell can improve its solar cell efficiency by modifying the incident solar spectrum. Ideally, all blue (UV) photons are converted to NIR photons, and the maximum possible photoluminescence quantum yield (PLQY) is 100%. However, there is another possibility. If the host bandgap is greater than twice the Yb^{3+} $^2F_{5/2} \rightarrow {}^2F_{7/2}$ electronic transition, the energy transfer from the host to Yb^{3+} can be via quantum cutting, a process wherein one UV-blue photon is converted to two NIR

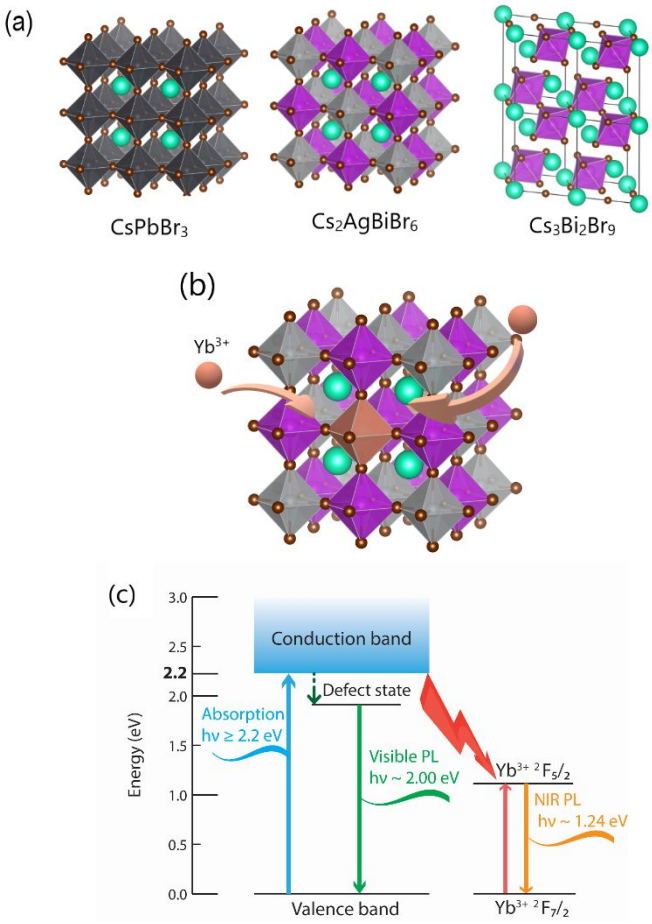

Fig. 1 (a) Structures of cubic $CsPbBr_3$ (#221, $Pm\bar{3}m$), cubic $Cs_2AgBiBr_6$ (#225, $Fm\bar{3}m$), and trigonal $Cs_3Bi_2Br_9$ (#164, $P\bar{3}m1$). (b) Yb^{3+} may substitute Ag^+ and Bi^{3+} ions in the octahedra in $Cs_2AgBiBr_6$. (c) Energy transfer processes in Yb-doped $Cs_2AgBiBr_6$.

[a] *Department of Chemical and Biomolecular Engineering, Tandon School of Engineering, New York University, 6 Metrotech Centre, Brooklyn, New York 11201 USA*

† Electronic Supplementary Information (ESI) available: Calculation of the minimum photoluminescence quantum yield (PLQY) needed to increase efficiencies of typical solar cells; experimental details of film deposition and characterization; exciton Bohr radius estimation; additional XRD, Raman spectra, and SEMs showing the effects of deposition and post-annealing conditions and Yb-doping; additional data on the stability of PLQY. See DOI: 10.1039/x0xx00000x

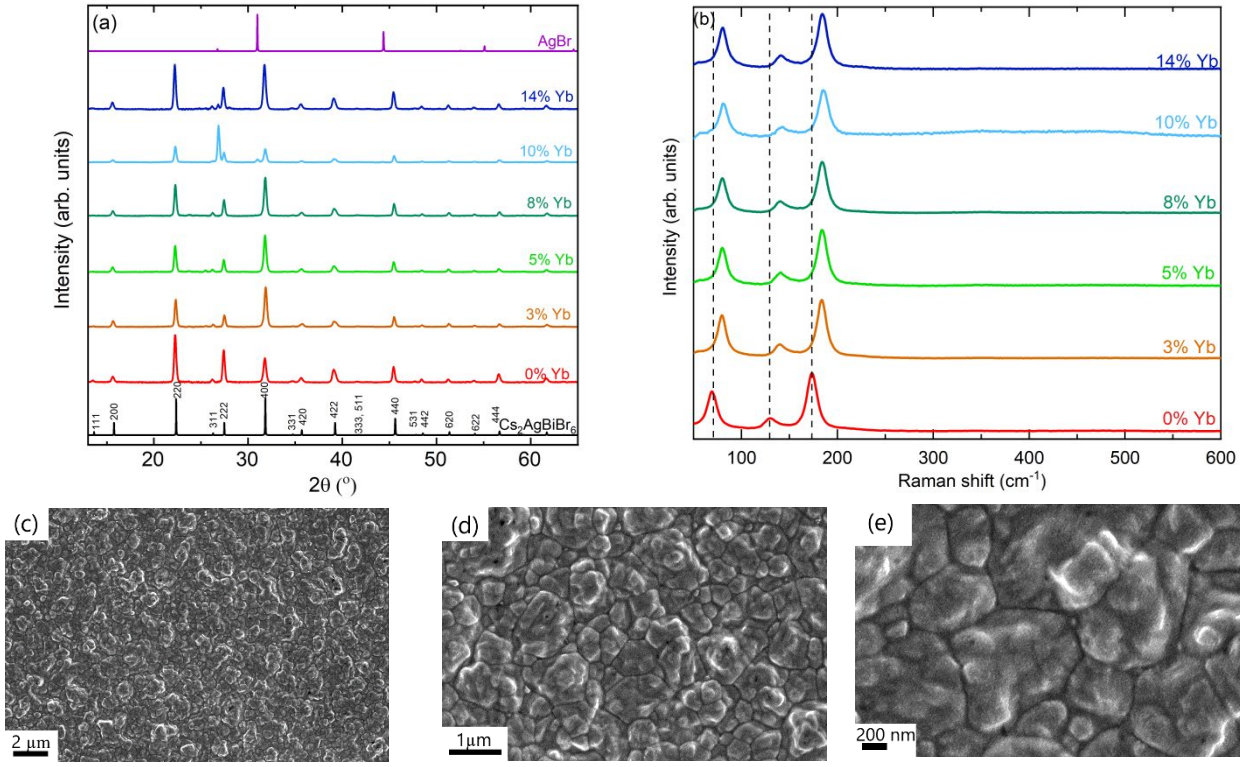

Fig. 2 (a) X-ray diffraction from Yb-doped $Cs_2AgBiBr_6$ films and simulated powder diffraction patterns of AgBr and $Cs_2AgBiBr_6$ for comparison. (b) Raman spectra of undoped and Yb-doped $Cs_2AgBiBr_6$ films. (c) - (e) Representative SEM images of Yb-doped (8%) $Cs_2AgBiBr_6$ films at different magnification. All data and images are from films annealed at 300 °C for one hour.

photons. In this case, PLQY can be >100% with a maximum of 200%. Indeed, Yb-doped $CsPbX_3$ (X=Cl, Br) have been shown to exhibit quantum cutting with PLQY as high as 190%.[2-5] However, lead is toxic, and NIR PLQY from $CsPbX_3$ decreases at high photon fluence.[4] In the search for non-toxic alternatives to $CsPbX_3$, double and bismuth-based perovskites are emerging as promising hosts because they have high absorption coefficients and tunable bandgaps in the visible range.[6-9] Specifically, Yb doping of $Cs_3Bi_2Br_9$, $Cs_2AgInCl_6$, and $Cs_2AgBiBr_6$[10-14] has been reported. Unfortunately, 28%, the highest PLQY from Yb-doped $Cs_2AgBiBr_6$ thin film,[13] is still much lower than the minimum PLQY estimated to increase solar cell efficiencies (69% for typical Si solar cells and 67% for typical CIGS solar cells, see ESI†). Herein, we report Yb-doped $Cs_2AgBiBr_6$ films with a maximum NIR PLQY of 82.5% and PLQY consistently in the 71-82.5% range for excitation energies above the bandgap (>2.2 eV), the highest values to date from a Yb-doped lead-free perovskite.

The double perovskite, $Cs_2AgBiBr_6$, crystallizes in a stable cubic structure (#225, $Fm\bar{3}m$, a=11.2499 Å) at room temperature.[15] The structure can be viewed as a derivative of the widely studied $CsPbBr_3$, wherein the Pb^{2+} in alternating $[PBr6]^{4-}$ octahedra are replaced by Ag^+ or Bi^{3+} forming a 3D network of corner-sharing $[AgBr_6]^{5-}$ and $[BiBr_6]^{3-}$ octahedra which alternate periodically (Fig. 1a). When $CsPbX_3$ is doped with Yb, Yb^{3+} is thought to substitute Pb^{2+} ions in the octahedra.[3] In $Cs_2AgBiBr_6$, Yb^{3+} would replace Bi^{3+} and Ag^+ ions when doped in $Cs_2AgBiBr_6$, as shown in Fig. 1b. Yb^{3+} substituting isovalent Bi^{3+} would not need to create a vacancy or an antisite defect, whereas substituting Ag^+ has to be accompanied by charge compensating defects such as Ag vacancies (V_{Ag}) or Ag antisite (Ag_{Bi}) defects.

We employed physical vapor deposition (PVD), specifically evaporation, to synthesize Yb-doped $Cs_2AgBiBr_6$ thin films from CsBr, $BiBr_3$, AgBr, and $YbBr_3$, whose evaporation rates were measured using separate quartz crystal microbalances. The details and the effects of deposition and annealing conditions are in the Supplementary Information (ESI†). Briefly, CsBr, $BiBr_3$, and AgBr evaporation rates and deposition durations were set to produce nominally stoichiometric $Cs_2AgBiBr_6$ with CsBr to $BiBr_3$ to AgBr molar flux ratios equal to 2:1:1. During the deposition of $Cs_2AgBiBr_6$ films, $BiBr_3$ (1.00 Å/s), AgBr (0.37 Å/s) and CsBr (1.21 Å/s) were co-evaporated onto glass substrates. For Yb-doped $Cs_2AgBiBr_6$ films, $BiBr_3$ (1.00 Å/s), AgBr (0.37 Å/s) and $YbBr_3$ (0.03-0.14 Å/s) were co-evaporated, while CsBr was deposited sequentially (1.21 Å/s). Each layer was deposited for 30 minutes, resulting in 490±10 nm thick films of $Cs_2AgBiBr_6$. The substrate temperature was not controlled and increased during the deposition. Films were annealed post-deposition on a hot plate in a nitrogen-filled glovebox at 250-350°C. Yb doping varied between 0% and 14% by controlling the $YbBr_3$ evaporation rate. The Yb concentration is reported as a percent of Bi lattice positions in stoichiometric $Cs_2AgBiBr_6$ (i.e., to deposit a 3% Yb-doped $Cs_2AgBiBr_6$ we set the ratio of $YbBr_3$ molar flux to $BiBr_3$ molar flux to 0.03.) All film characterizations were performed under ambient conditions. (Please see ESI† for details.)

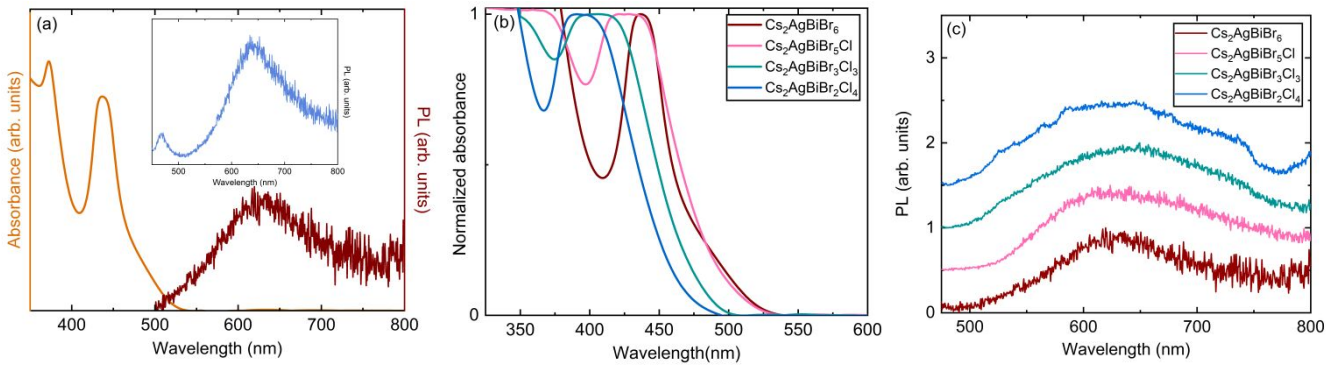

Fig. 3 (a) Absorbance and photoluminescence of $Cs_2AgBiBr_6$ thin film annealed at 300 °C for 1 hour. The inset is the PL from an as-deposited $Cs_2AgBiBr_6$ thin film. (b) Normalized absorbance and (c) PL from $Cs_2AgBiCl_yBr_{6-y}$ thin film thin film annealed at 300 °C for 1 hour. Thin-film interference fringes and background due to scattering were subtracted from the absorption spectra. The first exciton peaks in the $Cs_2AgBi(Br,Cl)_6$ absorbances shown in (b) are saturated (flat tops). Thinner films show a sharper absorption peak like that shown for $Cs_2AgBiBr_6$ but blueshifted due to Cl incorporation.

X-ray diffraction patterns of Yb-doped films annealed at 300 °C for one hour are shown in Fig. 2a. All films crystallize with the $Cs_2AgBiBr_6$ cubic structure (#225, $Fm\overline{3}m$). Annealing helps the precursors react completely and form the target $Cs_2AgBiBr_6$ structure. Otherwise, unreacted precursors (*e.g.,* AgBr) and other impurity phases, such as $Cs_3Bi_2Br_9$, are still present in the as-deposited films (Fig. S1, ESI†). We observe a small shift to higher 2θ values for Yb-doped films compared to the undoped $Cs_2AgBiBr_6$ film. Lattice parameters calculated from XRD data show a small unit cell contraction when Yb up to 10% is introduced to the perovskite structure (Table S1), which is reasonable because Yb^{3+} ions (101 pm) have a smaller radius than both Bi^{3+} (117 pm) and Ag^{+} (129 pm) ions.[16] Films with 10 and 14% Yb show XRD peaks from AgBr at 26.8° and 31.0°. One explanation is that Yb^{3+} substitutes the Ag^{+} ions, and the replaced silver forms AgBr as an impurity phase in the film. Another possibility is that adding Yb to $Cs_2AgBiBr_6$ destabilizes the structure and decomposes to AgBr and other impurity phases. Indeed, in addition to AgBr, we also detected Cs-Ag-Br ternary phases in our $Cs_2AgBiBr_6$ films when Yb concentration is 10% or greater (Fig. S2, ESI†). We attribute the reduction in AgBr diffraction peak from 10% Yb to 14% Yb to the increase in the fraction of these phases, which have overlapping XRD peaks with $Cs_2AgBiBr_6$ and, therefore, difficult to detect with XRD. However, they are detected with SEM/EDS (Fig. S2, ESI†). Creutz *et al.* reported the formation of AgBr and ternary Cs-Ag-Br phases as commonly observed impurity phases during colloidal synthesis of $Cs_2AgBiBr_6$. In our work, the Cs-Ag-Br impurity phases were more prevalent in as-deposited films and films annealed at 250 °C than at 300 °C (Fig. S2, ESI†). The $Cs_2AgBiBr_6$ films decompose at 350 °C, (Figs. S3 and S4, ESI†), making 300 °C a suitable optimized annealing temperature.

A comparison of Raman scattering from undoped and Yb-doped films confirmed ytterbium incorporation. Raman spectrum of an undoped $Cs_2AgBiBr_6$ film consists of three peaks at 173, 130, and 69 cm^{-1} (Fig. 2b), which agrees well with the reported Raman spectra.[17,18] Three vibrational modes, A_{1g}, E_g, and T_{2g}, either of $[BiBr_6]^{3-}$ or of $[AgBr_6]^{5-}$ octahedra, have been assigned to the peaks at 173, 130, and 69 cm^{-1}, respectively.[17,18] Doping $Cs_2AgBiBr_6$ with Yb shifts these peaks to higher wavenumbers: 69 to 80, 130 to 140, and 173 to 184 cm^{-1} at 14% Yb. Since Raman peaks shift to higher wavenumbers when the structure is compressed, the observed shifts in Yb-doped films confirm that Yb^{3+} ions substitute the octahedral cations in the perovskite structure, creating compression strain on the unit cell. Raman spectra from the annealed films do not show any impurity phase peaks (Fig. 2b). In contrast, Raman spectra from the as-deposited films show weak peaks assigned to $Cs_3Bi_2Br_9$ (Fig. S1, ESI†), suggesting that the impurity phases are present in the as-deposited films, but they are below the detection limit of Raman scattering in films annealed at 300 °C if they exist.

Scanning electron microscopy (SEM) images of annealed Yb-doped $Cs_2AgBiBr_6$ films show uniform films with grain sizes of a few hundred nanometers (Figs. 2c-e and Fig. S5, ESI†). As-deposited films contain poorly-defined small (<100 nm) $Cs_2AgBiBr_6$ grains and larger domains with different morphology and composition (Fig. S2, ESI†) consistent with unreacted precursors and impurity phases. During annealing, the $Cs_2AgBiBr_6$ grains grow and become more well-defined while the unreacted precursors and impurity phases are converted to $Cs_2AgBiBr_6$ and disappear. Compositional analysis by EDS also indicates the presence of Yb in the films. For example, the composition of 8% Yb-$Cs_2AgBiBr_6$ film is 0.6% Yb, 9.2% Bi, 10.3% Ag, 18.5% Cs and 61.4% Br, close to the values expected from the precursor fluxes (0.8% Yb, 9.7% Bi, 9.7% Ag, 19.4% Cs and 60.5% Br). In summary, XRD, Raman, and SEM-EDS data show that up to 14% of Yb was incorporated into the $Cs_2AgBiBr_6$ film while the perovskite host's cubic structure is still maintained.

Figure 3a shows the absorption and PL spectra of an undoped $Cs_2AgBiBr_6$ thin film. The absorption starts rising at 560 nm, suggesting a bandgap of ~ 2.2 eV, in the reported range of 1.8-2.3 eV for the indirect bandgap of this material.[15,17-26] The absorption peak at 435 nm matches reported data for nanocrystals,[6,22,24,27] and thin films.[19,26,28,29] In contrast, absorption measured on single crystals rises monotonically without any peaks,[15,17,18] likely a result of absorption saturation for thick samples. The absorption peak at 435 nm has been attributed to an exciton,[19,25-27,29] or the s-p transition on Bi.[22,23,28] The main objection to assigning this feature to an exciton has been the lack of a blue shift in its wavelength as

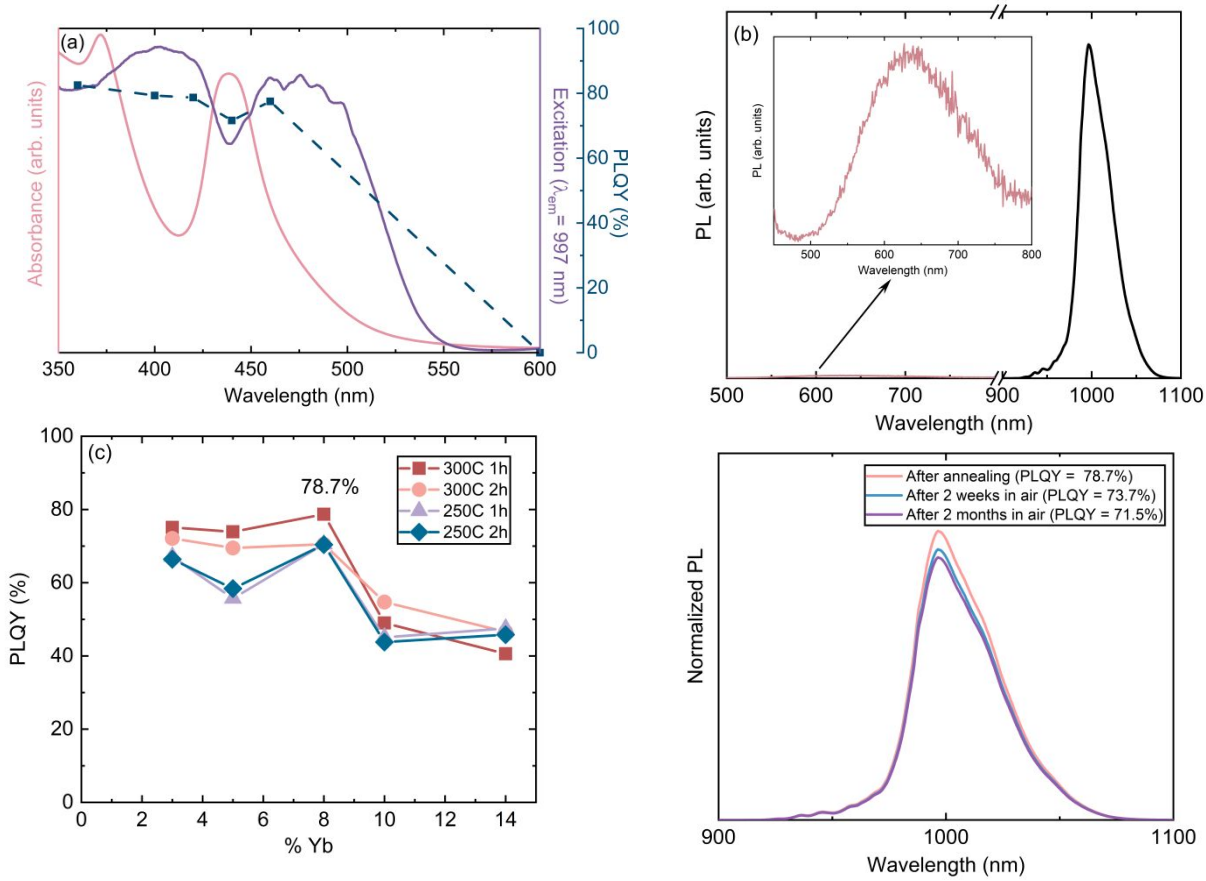

Fig. 4 (a) Absorption and excitation (λ_{em} = 997 nm) spectra of $Cs_2AgBiBr_6$ thin film doped with 8% Yb and annealed at 300 °C for 1 hour. NIR PLQY at different excitation wavelengths (squares) is also plotted. (b) Orange and NIR PL from $Cs_2AgBiBr_6$ thin film doped with 8% Yb and annealed at 300 °C for 1 hour. (c) NIR PLQY of $Cs_2AgBiBr_6$ films doped with 3-14% Yb annealed under different conditions. (d) Long-term stability of the PLQY of $Cs_2AgBiBr_6$ films doped with 8% Yb and annealed at 300 °C for one hour. Normalized PL means the intensity is scaled with the corresponding quantum yield. PL was excited at 420 nm (5nm bandwidth).

nanocrystal size is reduced (quantum confinement effect).[22,23] However, we do not expect $Cs_2AgBiBr_6$ to exhibit absorption blue-shift due to quantum confinement because the exciton Bohr radius in $Cs_2AgBiBr_6$ is estimated between 0.3 to 0.5 Å, smaller than one $Cs_2AgBiBr_6$ unit cell (Bohr radius calculation is included in ESI†). Interestingly, $Cs_3Bi_2Br_9$, with a corner-shared $[BiBr_6]^{3-}$ octahedra, also has an exciton absorption peak at 435 nm, associated with the localized exciton on $[BiBr_6]^{3-}$ octahedra.[10] The similarity between the two structures and their absorption features suggests that the $Cs_2AgBiBr_6$ absorption peak at 435 nm is also associated with localized excitons on the $[BiBr_6]^{3-}$ octahedra.

Photoluminescence (PL) from the undoped $Cs_2AgBiBr_6$ thin film is weak and comprises a broad emission centered around 630 nm (FWHM = 150 nm) (Fig. 3a). This broad emission has been observed in multiple studies,[15,17,18,22-24,26] but the origin is still under debate:[30] it has been associated with band-edge transition,[15,22] self-trapped excitons,[17,19,24,25] and defect-related recombination.[15,17,22,26] We deposited $Cs_2AgBiCl_yBr_{6-y}$ and shifted the bandgap of $Cs_2AgBiBr_6$ to higher energies by substituting bromine with chlorine to examine the origin of this orange PL. XRD patterns from $Cs_2AgBiCl_yBr_{6-y}$ thin films indicate that the halides are mixed throughout the films (Fig. S6, ESI†). As shown in Fig. 3b, the blue absorption peak shifts from 435 nm for y = 0 to 393 nm for y = 4 as the bandgap increases with chlorine substitution. However, the orange emission does not shift and remains centered at ~630 nm for all $Cs_2AgBiCl_yBr_{6-y}$ films (Fig. 3c). The intensity decreases with annealing (Fig. S7, ESI†). The lack of shift and decreasing intensity with annealing strongly suggests that the 630 nm emission originates from defects and is not due to a band-to-band transition. There is also a weak emission peak at 470 nm from the as-deposited undoped $Cs_2AgBiBr_6$ thin-film, but it disappears after annealing (Fig. 3a). The disappearance with annealing supports a defect origin. This $Cs_2AgBiBr_6$ emission peak at 470 nm was observed and attributed to a defect-related bound exciton by Dey *et al.*.[24] $Cs_3Bi_2Br_9$ thin film also has an emission peak at ~470 nm, assigned to emission from excitons trapped on defects.[10] The fact that both $Cs_2AgBiBr_6$ and $Cs_3Bi_2Br_9$ thin films have an absorption peak at 435 nm and an emission peak at 470 nm indicates that the absorption and subsequent emission have a common origin and are associated with excitons forming via light absorption and then becoming trapped and recombining on defects. The obvious candidate is a localized exciton on $[BiBr_6]^{3-}$ octahedra, forming upon light absorption and then getting trapped on a Bi vacancy, V_{Bi}, before emission. Cation vacancies are a feature of the $Cs_3Bi_2Br_9$ vacancy-ordered perovskite structure, so the 470 nm emission persists even after

annealing. $Cs_2AgBiBr_6$, on the other hand, is not a vacancy-ordered compound with Bi^{3+} and Ag^+ filling all octahedra. Therefore, any vacancies that may have formed during $Cs_2AgBiBr_6$ deposition would be expected to be filled, and vacancy concentration decrease as the films are annealed. Hence, the weak 470 nm emission associated with exciton recombination on Bi vacancies disappears after annealing.

Doping Yb into $Cs_2AgBiBr_6$ did not affect the optical absorption significantly. Yb-doped $Cs_2AgBiBr_6$ thin films still have an absorption peak at 435 nm, with the onset at ~560 nm (Fig. 4a), and the bandgap remains unchanged. The energy transfer from the $Cs_2AgBiBr_6$ host to the Yb^{3+} is efficient, and all films doped with Yb emit strongly in the NIR (1.24 eV), much stronger than the weak orange emission from the perovskite host (Fig. 4b and Fig. S8, ESI†.) The NIR emission peak is centered at 997 nm (FWHM = 40 nm), the expected Yb^{3+} $^2F_{5/2}\rightarrow$ $^2F_{7/2}$ electronic transition wavelength. Near-infrared PLQY depends strongly on the Yb concentration and annealing temperature. Films annealed at 300°C have the highest PLQY, and their PLQYs are stable with time in ambient air (Fig. 4d and Table S2). PLQY of films annealed at 250 °C decreases significantly after exposure to air (Table S2, ESI†). Fig. 4c shows that increasing the annealing time does not affect PLQY significantly; the difference in PLQY between films annealed for 1 hour and 2 hours is negligible for both annealing temperatures, 250 and 300°C. As shown in Fig. 4c and Fig. S9 (ESI†), we achieve high near-infrared PLQY between 73.9 and 78.7% for films doped with 3 to 8% Yb (excitation wavelength was 420 nm with 5 nm bandwidth). Near-infrared emission decreases sharply when Yb concentration is higher than 8%, with PLQY reducing to 40.6% for films with 14% Yb (Fig. 4c). This decrease in PLQY coincides with impurity peaks appearing in XRD of the films with 10 and 14% Yb. One possibility is that impurity phases and defect states introduce nonradiative relaxation pathways that compete with the energy transfer to Yb, decreasing the NIR emission. Another possibility for decreasing NIR emission with increasing Yb^{3+} concentration is the concentration quenching effect, wherein the excitation energy transfers from one Yb^{3+} to another and eventually to a defect where a nonradiative process quenches it. Concentration quenching should become important when Yb^{3+} ions are close to each other to allow energy transfer and typically above a threshold concentration.[31-33]

Previously, Schmitz *et al.* achieved 28% PLQY in $Cs_2AgBiBr_6$ with just 0.04% atomic substitution of Bi^{3+} with Yb^{3+} using hydrothermal synthesis.[13] They reported not being able to exceed this level of doping even after attempting to put as much as 20% Yb^{3+} into Bi^{3+} lattice positions. The challenge with hydrothermal synthesis may have been related to the widely discussed difficulty of doping colloidal nanocrystals during solution synthesis.[34] It has been shown that doping efficiencies in solution synthesis depend on dopant adsorption during growth which may be slow depending on surface morphology, nanocrystal shape, and surfactants in the growth solution. Thus, doping during hydrothermal synthesis may be kinetically limited. In contrast, nearly all the evaporated material condenses and reacts on the substrate surface in thermal evaporation. Thus, the dopant concentrations that can be incorporated into the film are limited by the thermodynamic solubility of the dopant in the host material. Based on cation sizes, Yb^{3+} is expected to have high solubility in $Cs_2AgBiBr_6$ and Figs. 2a and 2b show that at least up to 8% Yb^{3+} can be incorporated without any significant impurity phases appearing. What is surprising is that just 0.04% Yb was enough in hydrothermal synthesis to achieve 28% PLQY. In this work, PLQY is approximately three times that value but the Yb^{3+} concentrations are much, two orders of magnitude, higher. Clearly, not all Yb^{3+} in our films are active, and perhaps not all are needed, as evidenced by relatively flat (between 2% and 8% and eventually decreasing) PLQY with increasing Yb concentration.

Figure 4a shows the excitation spectrum of the $Cs_2AgBiBr_6$ film doped with 8% Yb and annealed at 300 °C for 1 hour (emission wavelength, λ_{em}= 997 nm). This film had the highest PLQY, 78.7%, when excited at 420 nm. Figure 4a also shows the absorption spectrum and PLQY measured at different excitation wavelengths (Fig. 4a). The excitation spectrum starts rising at 560 nm, the absorption onset, thus confirming that Yb^{3+} ions are not excited by the incident photons but receive energy from the perovskite host, as illustrated in Fig. 1c. When a photon with an energy higher than the $Cs_2AgBiBr_6$ bandgap (~2.2 eV, or wavelengths lower than 560 nm) is absorbed by the perovskite, it creates an electron-hole pair with the electron being excited to the conduction band. When the electron recombines with the hole, it transfers energy to a nearby Yb^{3+} ion. Electrons in Yb^{3+} ions are excited from the $^2F_{7/2}$ to the $^2F_{5/2}$ state and then emit in the NIR region when they relax down to the $^2F_{7/2}$ state. Thus, a UV-visible photon is downconverted to a NIR photon via the energy transfer from $Cs_2AgBiBr_6$ to Yb^{3+} ions (Fig. 1c). Interestingly, the excitation spectrum dips at 435 nm, where the exciton absorption peaks. However, PLQY remains high, 71.6%, when the film is excited at 440 nm. PLQY reaches the highest value of 82.5% when $Cs_2AgBiBr_6$ films doped with 8% Yb and annealed at 300 °C for 1 hour are excited at 360 nm. Depositing a layer of a downconversion material with 82.5% PLQY can increase a typical Si solar cell's efficiency from 20.3 to 20.6%, and a CIGS solar cell's efficiency from 20.4 to 20.7% (Fig. S10 and ESI† for calculations). Further optimization of the bandgap values and electronic structure by substituting Br with Cl or Bi with In and increasing the PLQY can lead to greater gains. For instance, whether there is quantum cutting in this material and whether PLQY can be increased above 100% remains an open question for future studies.

Finally, films annealed at 300 °C are stable in the air, and PLQY does not change significantly with time: PLQY of $Cs_2AgBiBr_6$ film doped with 8% Yb retains 94% of the PLQY after two weeks and 91% after two months without any encapsulation (Fig. 4d).

Conclusions

In summary, we synthesized undoped and Yb-doped $Cs_2AgBiBr_6$ thin films via PVD and showed efficient energy transfer from the host to the Yb^{3+} ions, which emits 1.24 eV NIR radiation with

efficiencies as high as 82.5%. PLQY of $Cs_2AgBiBr_6$ films doped with 8% Yb and annealed post-deposition at 300 °C remains high even after two months in the air. The perovskite host, $Cs_2AgBiBr_6$, has an exciton absorption centered at 435 nm, and the bandgap is estimated as 2.2 eV. The weak and broad emission at 630 nm is assigned to defect recombination. Using the record efficiencies reported here as a starting point, further improvements in synthesis conditions of this class of lead-free materials are likely to increase their PLQY towards 100%. This creates new prospects for modifying the solar spectrum by spectrum shifting to increase solar cell efficiencies.

Acknowledgments

The authors thank Dr. Jason A. Röhr for helpful discussions. The X-ray microdiffractometer with GADDS was acquired through the support of the National Science Foundation under Award Numbers CRIF/CHE-0840277 and the NSF MRSEC Program under Award Number DMR-0820341. In addition, the authors acknowledge the use of shared facilities provided through the Materials Research Science and Engineering Center (MRSEC) and MRI programs of the National Science Foundation under Award Numbers DMR-1420073 and DMR-0923251.

Conflicts of interest

The authors and New York University have filed a provisional patent based on the information in this article.

References

1 M. Gloeckler and J. R. Sites, *J. Phys. Chem. Solids,* 2005, **66**, 1891-1894.
2 G. Pan, X. Bai, D. Yang, X. Chen, P. Jing, S. Qu, L. Zhang, D. Zhou, J. Zhu, W. Xu, B. Dong and H. Song, *Nano Lett*., 2017, **17**, 8005-8011.
3 T. J. Milstein, D. M. Kroupa and D. R. Gamelin, *Nano Lett*., 2018, **18**, 3792-3799.
4 D. M. Kroupa, J. Y. Roh, T. J. Milstein, S. E. Creutz and D. R. Gamelin, *ACS Energy Lett*., 2018, **3**, 2390-2395.
5 M. J. Crane, D. M. Kroupa, Y. J. Roh, R. Y. Anderson, M. D. Smith and D. R. Gamelin, *ACS Appl. Energy Mater*., 2019, **2**, 4560-4565.
6 S. E. Creutz, E. N. Crites, M. C. De Siena and D. R. Gamelin, *Nano Lett*., 2018, **18**, 1118-1123.
7 M. B. Gray, E. T. McClure and P. M. Woodward, *J. Mater. Chem. C*, 2019, **7**, 9686-9689.
8 S. E. Creutz, H. Liu, M. E. Kaiser, X. Li and D. R. Gamelin, *Chem. Mater.* 2019, **31**, 4685-4697.
9 M. N. Tran, I. J. Cleveland and E. S. Aydil, *J. Mater. Chem. C.* 2020, **8**, 10456-10463.
10 M. N. Tran, I. J. Cleveland, G. A. Pustorino and E. S. Aydil, *J. Mater. Chem. A*, 2021, **9**, 13026-13035.
11 W. Lee, S. Hong and S. Kim, *J. Phys. Chem. C*, 2019, **123**, 2665–2672.
12 Y. Mahor, W. J. Mir and A. Nag, *J. Phys. Chem. C*, 2019, **123**, 15787-15793.
13 F. Schmitz, K. Guo, J. Horn, R. Sorrentino, G. Conforto, F. Lamberti, R. Brescia, F. Drago, M. Prato, Z. He, U. Giovanella, F. Cacialli, D. Schlettwein, D. Meggiolaro and T. Gatti, *J. Phys. Chem. Lett.* 2020, **11**, 8893−8900.
14 N. Chen, T. Cai, W. Li, K. Hills-Kimball, H. Yang, M. Que, Y. Nagaoka, Z. Liu, D. Yang, A. Dong, C. Y. Xu, R. Zia and O. Chen, *ACS Appl. Mater. Interfaces.,* 2019, 11, **18**, 16855–16863.
15 A. H. Slavney, T. Hu, A. M. Lindenberg and H. I. Karunadasa, *J. Am. Chem. Soc*., 2016, **138**, 2138−2141.
16 R. D. Shannon, *Acta Crystallogr A*, 1976, **32**, 751-767.
17 S. Zelewski, J. M. Urban, A. Surrente, D. K. Maude, A. Kuc, L. Schade, R. D. Johnson, M. Dollmann, P. K. Nayak, H. J. Snaith, P. Radaelli, R. Kudrawiec, R.J. Nicholas, P. Plochocka and M. Baranowski, *J. Mater. Chem. C*, 2019, **7**, 8350-8356.
18 J. A. Steele, P. Puech, M. Keshavarz, R. Yang, S. Banerjee, E. Debroye, C. W. Kim, H. Yuan, N. H. Heo, J. Vanacken, A. Walsh, J. Hofkens and M. B. J., Roeffaers, *ACS Nano.* 2018, **12** (8), 8081-8090.
19 R. Kentsch, M. Scholz, J. Horn, D. Schlettwein, K. Oum and T. Lenzer, J. Phys. Chem. C, 2018, 122, 25940-25947.
20 M. R. Filip, S. Hillman, A. A. Haghighirad, H. J. Snaith and F. Giustino, *J. Phys. Chem. Lett*., 2016, **7**, 2579−2585.
21 E. T. McClure, M. R. Ball, W. Windl and P. M. Woodward, *Chem. Mater*., 2016, **28**, 1348−1354.
22 Y. Bekenstein, J. C. Dahl, J. Huang, W. T. Osowiecki, J. K. Swabeck, E. M. Chan, P. Yang and A. P. Alivisatos, *Nano Lett.,* 2018, **18**, 3502−3508.
23 F. Igbari, R. Wang, Z.-K. Wang, X.-J. Ma, Q. Wang, K.-L. Wang, Y. Zhang, L. S. Liao and Y. Yang, *Nano Lett.,* 2019, **19**, 2066−2073.
24 A. Dey, A. F. Richter, T. Debnath, H. Huang, L. Polavarapu and J. Feldmann, *ACS Nano*., 2020, **14**, 5855−5861.
25 M. Palummo, E. Berrios, D. Varsano and G. Giorgi, *ACS Energy Lett*., 2020, **5**, 457−463.
26 A. D. Wright, L. R. V. Buizza, K. J. Savill, G. Longo, H. J. Snaith, M. B. Johnston and L. M. Herz, *J. Phys. Chem. Lett.,* 2021, **12**, 3352−3360.
27 B. Yang, J. Chen, S. Yang, F. Hong, L. Sun, P. Han, T. Pullerits, W. Deng and K. Han, *Angew. Chem. Int. Ed*., 2018, **57**, 5359 – 5363.
28 M. Wang, P. Zeng, S. Bai, J. Gu, F. Li, Z. Yang and M. Liu, *Sol. RRL*., 2018, **2**, 1800217.
29 C. Wu, Q. Zhang, Y. Liu, W. Luo, X. Guo, Z. Huang, H. Ting, W. Sun, X. Zhong, S. Wei, S. Wang, Z. Chen and L. Xiao, *Adv. Sci*., 2018, **5**, 1700759.
30 G. Longo, S. Mahesh, L. R. V. Buizza, A. D. Wright, A. J. Ramadan, M. Abdi-Jalebi, P. K. Nayak, L. M. Herz and H. J. Snaith, *ACS Energy Lett*. 2020, **5**, 2200−2207.
31 D. L. Dexter, *J. Chem. Phys.* 1954, **22**,1063-1070.
32 Z. Song, J. Zhao and Q. Liu, *Inorg. Chem. Front.* 2019, **6**, 2969-3011.
33 F. Zhao, H. Cai, Z. Song and Q. Liu, *Chem. Mater.* 2021, **33**, 8360-8366.
34 S. C. Erwin, L. J. Zu, M. I. Haftel, A. L. Efros, T. A. Kennedy and D. J. Norris, *Nature* 2005, **436**, 91-94.